Bull Volcanol (2000) 62 : 20–33 © Springer-Verlag 2000

RESEARCH ARTICLE

**J. E. Gardner · S. Tait**

# The caldera-forming eruption of Volcán Ceboruco, Mexico

Received: 18 November 1998 / Accepted: 23 October 1999

**Abstract** Volcán Ceboruco (Mexico) erupted ~1000 years ago, forming a caldera ~4 km in diameter. The pyroclastic deposit (Jala pumice) produced was studied at 75 sites, where thicknesses of all tephra layers were measured and, at many sites, the five coarsest lithics in each fall layer were measured. Several fall layers were also sieved for component analysis. White (rhyodacite) and gray (dacite) pumices occur in every tephra layer. The eruption began by dispersing a thin, narrowly distributed fall layer (P0) to the north. Next, a widely dispersed, coarse, Plinian fall deposit (P1), the most voluminous layer in the Jala pumice, erupted. The rest of the eruption alternated between pyroclastic surges and flows (including the Marquesado pyroclastic flow, southwest of the volcano) and Plinian falls (P2–P6). In all, 3–4 $km^3$ of magma erupted, ~95% of which was deposited as fall layers. During most of the deposition of P1, eruptive intensity (mass flux) was almost constant at 4–8×$10^7$ kg $s^{-1}$, producing a Plinian column 25–30 km in height. Size grading at the top of P1 indicates, however, that mass flux waned dramatically, and possibly that there was a brief pause in the eruption. During the post-P1 phase of the eruption, a much smaller volume of magma erupted, although mass flux varied by more than an order of magnitude. We suggest that caldera collapse began at the end of the P1 phase of the eruption, because along with the large differences in mass flux behavior between P1 and post-P1 layers, there were also dramatic changes in lithic content (P1 contains ~8% lithics; post-P1 layers contain 30–60%) and magma composition (P1 is 98% rhyodacite; post-P1 layers are 60–90% rhyodacite). However, the total volume of magma erupted during the Jala pumice event is close to that estimated for the caldera. These observations appear to conflict with models which envision that, after an eruption is initiated by overpressure in the magma chamber, caldera collapse begins when the reservoir becomes underpressurized as a result of the removal of magma. The conflict arises because firstly, the P1 layer makes up too large a proportion (~75%) of the total volume erupted to correspond to an overpressurized phase, and secondly, the caldera volume exceeds the post-P1 volume of magma by at least a factor of three. The mismatches between model and observations could be reconciled if collapse began near the beginning of the eruption, but no record of such early collapse is evident in the tephra sequence. The apparent inability to place the Jala pumice eruptive sequence into existing models of caldera collapse, which were constructed to explain the formation of calderas much greater in volume than that at Ceboruco, may indicate that differences in caldera mechanics exist that depend on size or that a more general model for caldera formation is needed.

**Key words** Caldera eruptions · Tephrostratigraphy · Caldera collapse · Volcán Ceboruco · Marquesado pyroclastic flow

Editorial responsibility: W. Hildreth

James E. Gardner (✉)
Department of Geological Sciences, Brown University, Providence, RI, USA
e-mail: gardner@gi.alaska.edu
Fax: +1-907-4745163

Steve Tait
Laboratoire de Dynamic des Systèmes Géologiques, Institut de Physique du Globe, 4 place Jussieu, F-75252 Paris cédex 05, France

*Present address:*
J. E. Gardner, Geophysical Institute, University of Alaska Fairbanks, Fairbanks, AK 99775-7320, USA

## Introduction

Most calderas form during specific volcanic eruptions (Williams 1941; Smith 1960, 1979; Smith and Bailey 1968). Smith (1979) observed that calderas range in

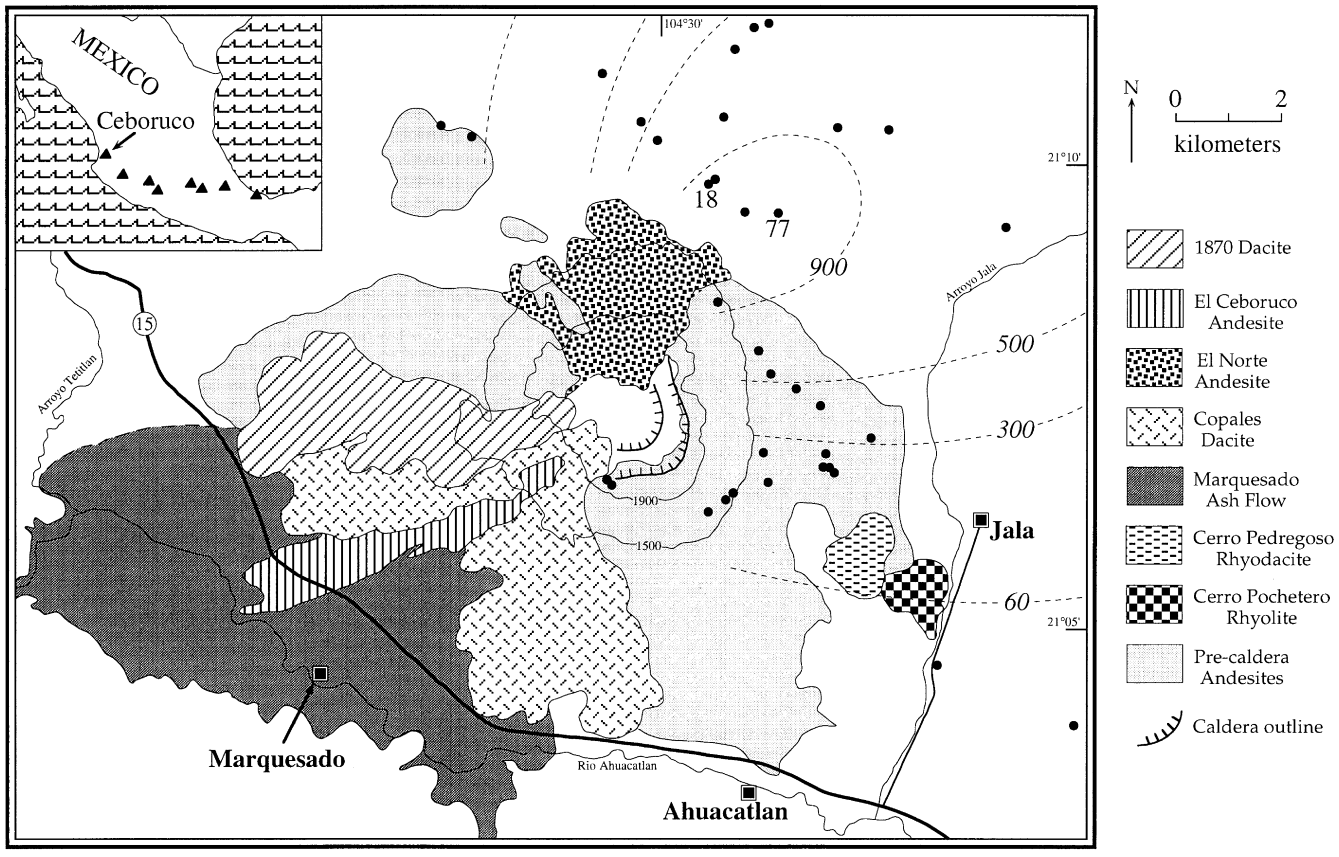


**Fig. 1** Simplified map of Volcán Ceboruco with present-day distributions of pre-caldera andesites and domes, Marquesado ash-flow deposits, outlines of inner and outer calderas, and some post-caldera andesites and dacites (modified from Nelson 1980). *Dotted curves* are proximal isopachs (in centimeters) of total Jala pumice thickness. Solid dots show positions of 35 sample sites of this study. Sieve samples were collected at site 18, and geochemical samples were collected at sites 18 and 77. The inner caldera is on the upper part of a dome that partially fills the outer caldera. *Inset* shows Volcán Ceboruco and other recently active volcanoes in Mexico

size from less than 1 $km^2$ to more than 1000 $km^2$, and that their size correlates with the volume of erupted pyroclastic material. One of the largest known calderas is the $85 \times 35$-km La Garita Caldera (San Juan Volcanic Field, USA), which formed when 5000 $km^3$ of magma erupted as the Fish Canyon Tuff (Steven and Lipman 1976; Lipman et al. 1997). Detailed studies of the eruptive deposits of, for example, Crater Lake and Valley of Ten Thousand Smokes, suggest that calderas start to collapse neither right at the beginning nor at the end of eruptions, but instead after a (relatively small) proportion of the total magma has erupted (Bacon 1983; Hildreth 1991; Suzuki-Kamata et al. 1993). Not all explosive volcanic eruptions, however, lead to caldera formation. The smallest eruptions that lead to caldera collapse seem to erupt approximately 1–10 $km^3$ of magma, such as the 1883 eruption of Krakatau and the 1991 eruption of Pinatubo (Sigurdsson et al. 1991; Paladio-Melosantos et al. 1996). On the other hand, neither the eruption of 4 $km^3$ from Quizapu (Chile) nor ~8.5 $km^3$ from Santa María (Guatemala) led to caldera collapse (Williams and Self 1983; Hildreth and Drake 1992). It seems that approximately 1–10 $km^3$ of magma needs to erupt before volcanoes founder to form calderas. Studies of relatively small volume eruptions that result in calderas may, therefore, help in understanding the conditions needed for collapse to occur.

This study focuses on one small-volume eruption, that of Volcán Ceboruco in Mexico (Fig. 1), that resulted in the formation of a caldera (Nelson 1980). As discussed herein, the tephra sequence (Jala pumice and Marquesado Pyroclastic Flow) formed during the eruption is somewhat unique in that more than 90% of the volume was deposited as Plinian fall layers. We describe the individual layers in the eruptive sequence, estimate their volumes, calculate mass eruption rates in the cases of the fall layers, and speculate as to when the caldera began to collapse.

Volcán Ceboruco, one of the westernmost volcanoes in the Mexican Volcanic Belt, is truncated by two concentric calderas (Fig. 1). Nelson (1980) studied the development of the volcano in detail. Herein we summarize his findings.

The main edifice was constructed by extrusion of ~60 $km^3$ of andesitic lava flows. This was followed by a relatively quiet period of undetermined length, when only two domes (the rhyodacitic Cerro Pedregoso and

the rhyolitic Cerro Pochetero) extruded on the lower flanks of the volcano (Fig. 1). Then, ~1000 years ago, the volcano erupted the Jala pumice and Marquesado pyroclastic flow deposits and collapsed to form the outer caldera. The Jala pumice sequence is a thick blanket of pumice fall and ash layers, deposited mostly to the northeast, whereas the Marquesado flows were deposited in the southwest. Following this eruption, a dacite dome extruded, partially filling the caldera. Further extrusions of lavas undermined the dome, causing it to partially collapse to form the inner caldera, which is ~1.5 km wide. Ensuing eruptions were mostly of andesitic lavas that cover the north and southwest flanks of the volcano. Most recently, the volcano erupted from 1870 to 1875 AD, first with small ash explosions and then extrusion of 1.1 $km^3$ of dacitic lava (summarized in Nelson 1980).

## Methods

### Field studies

The Jala pumice tephra sequence was examined at 75 sites, mostly north and east of the volcano (Fig. 1). At 59 of those sites the base of the sequence was exposed. The thickness of each tephra layer present at every site was measured. The coarsest lithic fragments were measured in many of the fall layers at most sites, by excavating a standard area of each layer and measuring the major axes of the five largest lithics found. Where deposits were sufficiently thick (usually >20 cm), they were subdivided and the largest lithics from each level were measured to determine the variation in size as a function of stratigraphic height.

A preliminary set of samples from the four most prominent fall layers were sieved to determine the relative proportions of pumice and lithic clasts. These samples were collected at Site 18, located 4 km north of the northern rim of the outer caldera (Fig. 1). Although the lithic content of a deposit varies with distance and direction from vent, relative differences between layers in the Jala pumice sequence do not, i.e., lithic-rich layers always have a greater abundance of lithics than do lithic-poor ones (Fig. 2). In addition, two pumice types, which appear white and dark gray in the field, occur in each layer and their relative proportions were determined in the sieve samples (Fig. 2). Mixing between white and gray material as banded pumices indicate that both magmas were molten at the time of the eruption. In our sieve samples, banded pumices were designated as white or gray, depending on which type was more abundant.

### Analytical studies

Bulk compositions of three white pumices and four gray pumices were determined by fusing each to a glass and analyzing them by electron microprobe (Table 1). This was done by pulverizing each pumice to a fine powder, individually wrapping the powders in Mo foil, and placing them inside separate silica tubes, which had been sealed at one end. These tubes were then vacuum evacuated, welded shut, and suspended inside a furnace at 1300 °C for 3 h. Thin sections were made of the fused glasses and analyzed using the Cameca Camebax electron microprobe at Brown University. Glass analyses were obtained using a 10-kV accelerating voltage, 10-nA beam current, and a defocused beam (~10-μm diameter), using techniques described by Devine et al. (1995). Precision

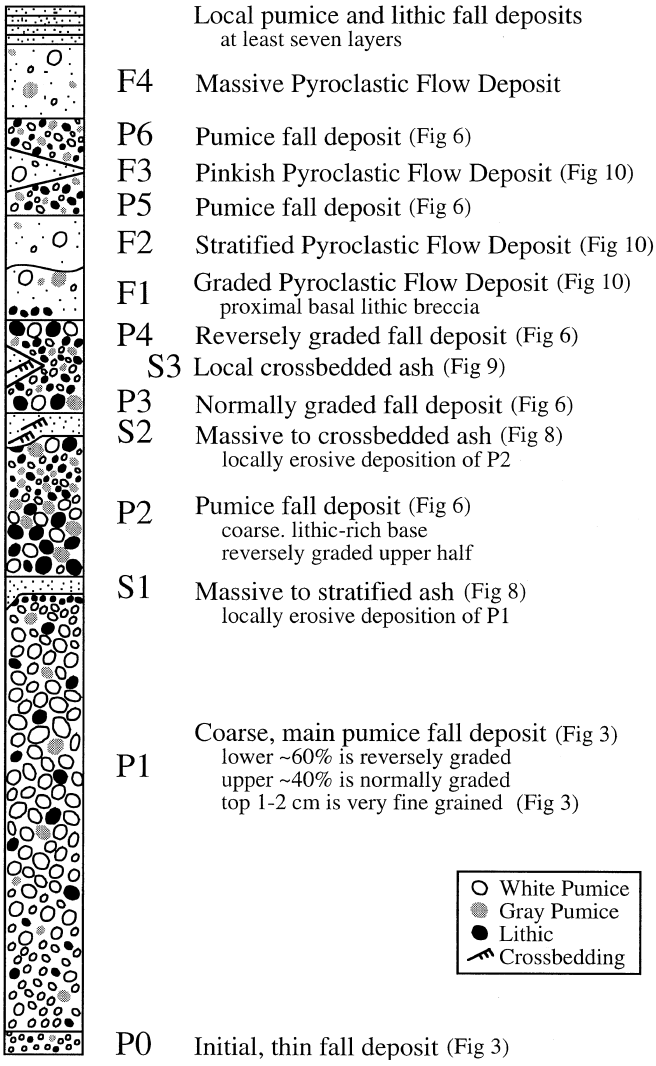


**Fig. 2** Schematic, composite stratigraphic column and brief descriptions of tephra layers in the Jala pumice sequence (thicknesses not to scale). Relative number and size of white and gray pumices and lithics highlight differences between layers. Figures showing distributions of the layers around Volcán Ceboruco are given in parentheses

**Table 1** Compositions of eruptive products of the Jala Pumice

| Site[a] | 18 | 18 | 18 | 77 | 77 | 77 | 77 |
|---|---|---|---|---|---|---|---|
| Pumice[b] | P1B-A | P1M-B | P1T-B | P2B-A | P2B-B | P2B-E | P2B-F |
| Type[c] | White | White | White | Gray | Gray | Gray | Gray |
| $SiO_2$[d] | 70.69 | 70.49 | 70.63 | 67.70 | 67.48 | 67.76 | 67.68 |
| $TiO_2$ | 0.27 | 0.28 | 0.30 | 0.47 | 0.51 | 0.47 | 0.47 |
| $Al_2O_3$ | 16.05 | 16.06 | 15.97 | 16.39 | 16.63 | 16.45 | 16.48 |
| FeO | 1.97 | 2.00 | 2.06 | 3.13 | 3.02 | 2.98 | 3.03 |
| MnO | 0.09 | 0.09 | 0.11 | 0.13 | 0.09 | 0.16 | 0.11 |
| MgO | 0.38 | 0.41 | 0.39 | 1.04 | 0.97 | 0.91 | 0.99 |
| CaO | 1.56 | 1.62 | 1.55 | 2.65 | 2.65 | 2.61 | 2.69 |
| $Na_2O$ | 5.72 | 5.81 | 5.66 | 5.61 | 5.68 | 5.69 | 5.53 |
| $K_2O$ | 3.27 | 3.25 | 3.32 | 2.88 | 2.98 | 2.98 | 3.02 |
| Total | 99.49 | 100.48 | 99.91 | 101.06 | 99.37 | 100.12 | 99.78 |

[a] Site where pumice was collected; see Fig. 1
[b] Pumice number: e.g., P1B-A represents layer P1, base, pumice A
[c] White pumice or gray pumice. None of the pumices analyzed were banded
[d] All data (in weight percent) are averages of six analyses per sample, normalized to 100% for comparative purposes. Original totals are listed. All Fe as FeO. See text for analytical techniques

and accuracy were monitored by repeatedly analyzing KN-18, a comendite obsidian. Thin sections were prepared of white, gray, and banded pumices for petrographic examination. Matrix glasses in many of these were analyzed using the above techniques. Phenocrysts were analyzed by electron microprobe, using a 15-kV accelerating voltage, 15-nA beam current, and a focused beam.

## Tephra stratigraphy of the Jala pumice

The stratigraphy of the Jala pumice consists of a thick pumice layer overlain by alternating pumice fall and ash layers (Fig. 2). Our main objective was to investigate the eruption characteristics of the fall phases of the eruption and so we focus our discussion on the fall deposits. We do not have grain-size data for the other ash layers, but their poorly sorted nature (pumice and lithic blocks set in fine ash matrix), internal stratigraphy, irregular distribution, and erosion of the underlying deposits suggest that they were deposited by pyroclastic flows or surges. Furthermore, some deposits have internal stratifications (crossbedding or lamination) which indicate they were deposited by pyroclastic surges. In our stratigraphic sequence, we designate fall layers with P (Fig. 2). We designate those layers that we believe, based on the above criteria, were pyroclastic surges with S, and flows with F. Subsequent numbers designate their relative order in the sequence, e.g., S1 is the first pyroclastic surge deposit.

### P0 fall layer

The first layer in the sequence is a thin, relatively fine-grained fall layer (Fig. 2). This layer forms a narrow lobe oriented approximately N35 °E, which extends no more than 5 km across axis, but its 10 cm isopach extends more than 20 km away from the volcano (Fig. 3). It is slightly reversely graded, and its lithic clasts are, on average, two to four times smaller than in the base of P1 (Fig. 4). P0 was not sieved but appears to contain ~10 wt.% gray pumice near the base and <5 wt.% toward the top.

### P1 fall layer

The main layer of the Jala pumice (P1; Fig. 2) is a thick blanket of well-sorted pumice and ash with a dispersal axis of approximately N70 °E. Approximately 5 km north of the volcano P1 is almost 7 m thick, and is still almost 1.5 m thick approximately 20 km away (Fig. 3). Nelson (1980) mentions some localities where P1 is thicker, but we found that at many of those sites P1 was deposited on a slope and overthickened by slumping and rolling during deposition. Samples from five stratigraphic heights in P1 were sieved and the percentage of lithics is ~8 wt.%, and are mostly fragments of andesitic lavas. Throughout P1, pumices are 98 wt.% white and 2 wt.% gray.

At most sites we find that maximum lithic size increases slightly in the lower ~60% of P1, whereas much of the upper ~40% of the deposit is normally graded, with maximum size decreasing by 10–15% (Fig. 4). This normal grading becomes extreme in the upper 1–4 cm of the deposit with sizes decreasing to roughly those in P0 (Fig. 5). This fine-grained top, which consists of well-sorted, small pumices with minor lithics, is thickest (up to 4 cm) at sites 5–10 km away from the volcano (Fig. 3). Nearer the volcano, it is usually 1–2 cm thick, but this is because it was partially eroded by a subsequent surge (S1; see below). This pumice layer appears as fine grained as P0, but it is dispersed as widely as the coarser part of P1 (Fig. 3). The fine pumice layer is overlain by a layer, up to 1 cm thick, of well-sorted, small lithics and minor amounts of pumice (Fig. 5). This lithic-rich layer has a dispersal similar to P0 (Fig. 3). Both the

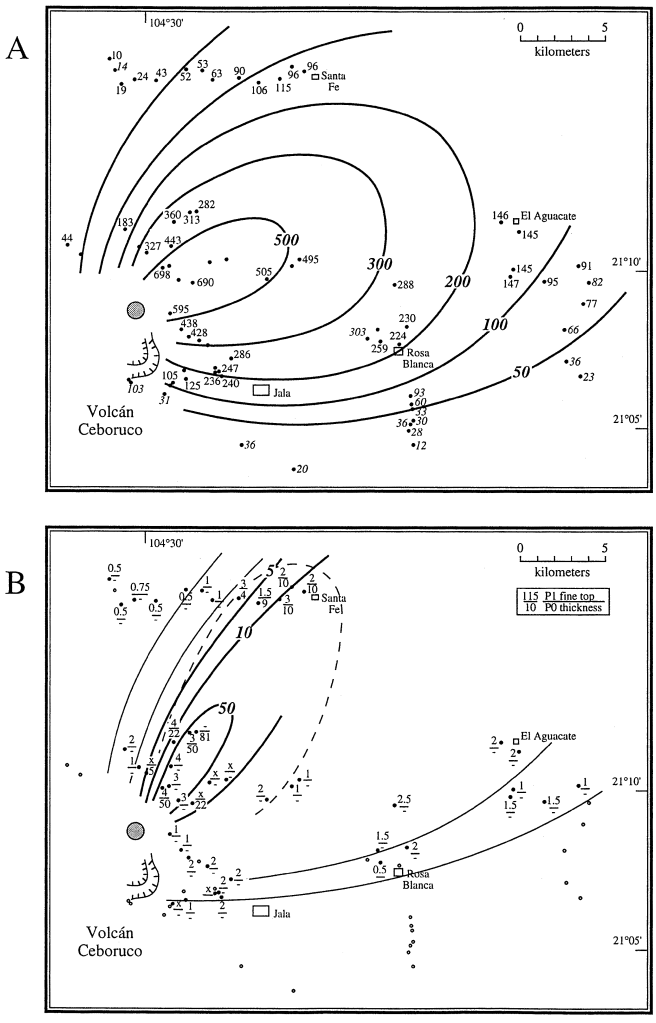


**Fig. 3** Isopachs (in centimeters) of **A** P1 pyroclastic fall layer and **B** P0 pyroclastic fall deposit (*thick lines*) and fine top of P1 (*thin lines*). *Italized numbers* for P1 indicate incomplete thicknesses because either the base was unexposed or the top was eroded. Thicknesses at each site in **B** are for the P1 top (*upper number*) and P0 (*lower number*); *dash* indicates that layer was not present and *x* indicates layer was present but not measured. *Dotted curve* outlines the sites where the top lithic-rich fall of P1 is found. Possible location of the Plinian vent is shown by *stippled circle* (see text)

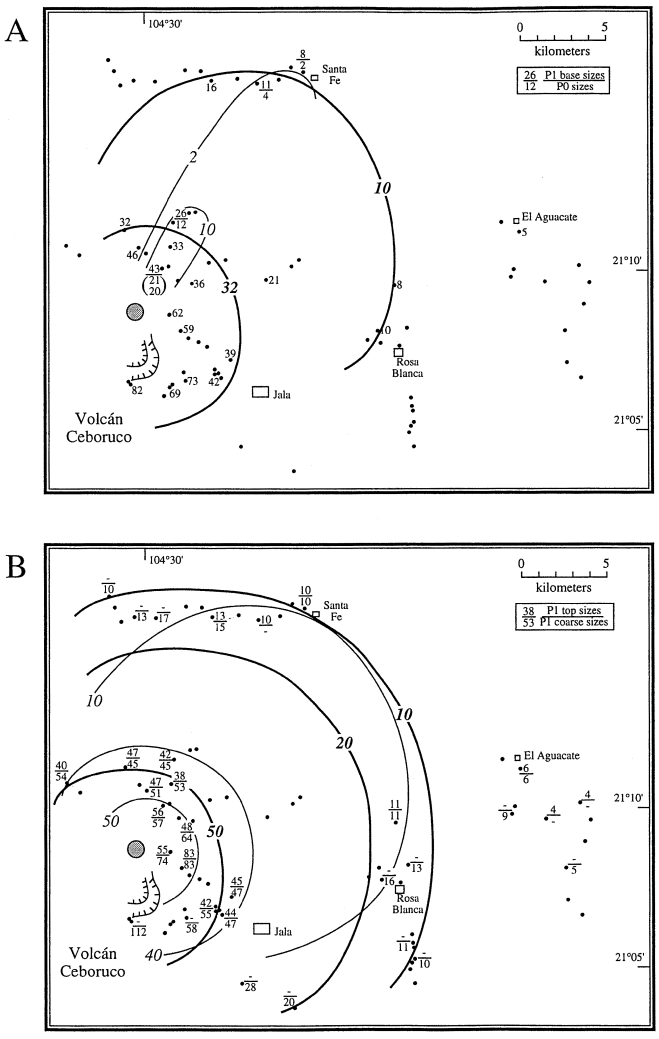


**Fig. 4** Lithic isopleths (in millimeters) for **A** P0 (*thin lines*) and the base of the P1 (*thick lines*), and **B** for the coarsest level of P1 (*thick lines*), which corresponds to 60% above the base at each site, and the top of P1 (*thin lines*), which does not include the fine-grained top. P0 was divided at one site (in parentheses); the *bottom number* is the lithic size for the lower 25 cm of the layer, and the *top number* is that for the upper 25 cm. All data are averages of the five largest lithic fragments at each site. Possible location of the Plinian vent is shown by *stippled circle* (see text)

fine pumice and fine lithic layers are most likely fall layers, and not related to deposition of the susequent surge S1, because they are well sorted, thin systematically with distance, and are present even where S1 is absent.

## P2 fall layer

The third fall layer in the sequence is P2 (Fig. 2). This layer was dispersed in approximately the same direction as P1, and is thickest ~5 km northeast of the volcano, where it reaches 170 cm (Fig. 6). P2 thins with distance, but is still 0.5 m thick on the outskirts of Santa Fe, 18 km north of the volcano. P2 is distinctly richer in lithic fragments and gray pumices relative to P1, making P2 easily distinguishable in the field.

There are internal stratifications in P2 that are present everywhere a complete section is found, and can be grouped into two units which are approximately equal in thickness (Fig. 2). The lower unit of P2 is, on average, 40% coarser than the upper half (Fig. 7). Within the lower unit lithic abundance decreases dramatically, from ~60 to ~30 wt.%, whereas maximum lithic size decreases, on average, by ~10%. The upper unit of P2 is strongly reversely

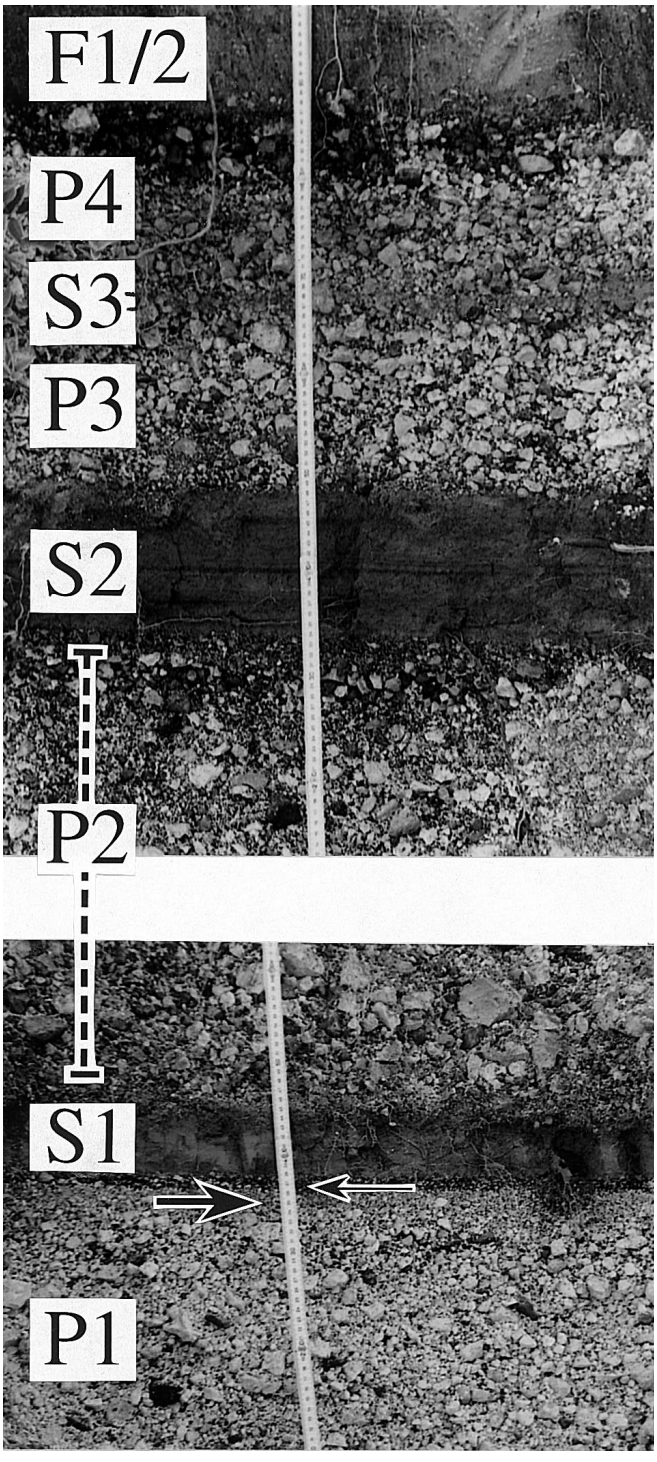


**Fig. 5** Photographs of deposits in the Jala pumice at site 18 (see Fig. 1). Shown are the top of *P1, S1,* bottom and top of *P2, S2, P3, S3, P4,* and the bottom of *F1/2* (see Fig. 2). Note the fine-grained top (*thick arrow*) overlain by a layer of fine-grained lithics (*thin arrow*) at the top of *P1.* Note also stratification in *S2.* At this site *S3* only occurs as a 2- to 3-cm band of fine-ash coating on pumices. Divisions on scale bar are in centimeters

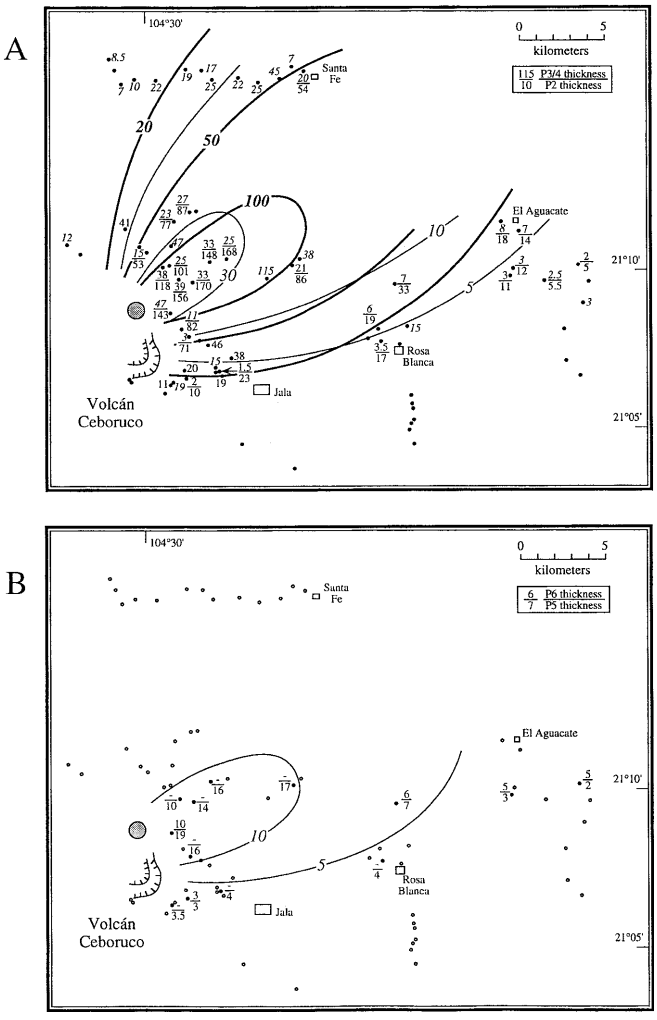


**Fig. 6** Isopachs (in centimeters) of **A** P2 pyroclastic fall deposit (*thick lines*) and of combined P3 and P4 pyroclastic fall deposits (*thin lines*). When only one value is given, it is for P2. *Italicized numbers* indicate incomplete thicknesses. P3 and P4 can only be clearly separated within approximately 5 km of Volcán Ceboruco. Isopachs (in centimeters) of **B** for the combined P5 and P6 pyroclastic fall layers. *Dash* indicates that P6 is missing. Possible location of the Plinian vent is shown by *stippled circle* (see text)

graded, with the lower part of the unit being as fine grained as P0 and then maximum lithic size increases by ~60%. Lithic content also increases from ~35 to ~45 wt.%. Near the volcano, the upper unit of P2 was eroded by the surge that overrode P2 and deposited S2 (see below).

## P3/4 fall layer

The next two fall deposits are mapped as one because they can only be clearly distinguished within 5 km of the volcano, where they are separated by S3 (Fig. 2). The full thickness of P3/4 is preserved in only a few areas. More often the thickness has been eroded by either overlying pyroclastic flows (near the volcano)

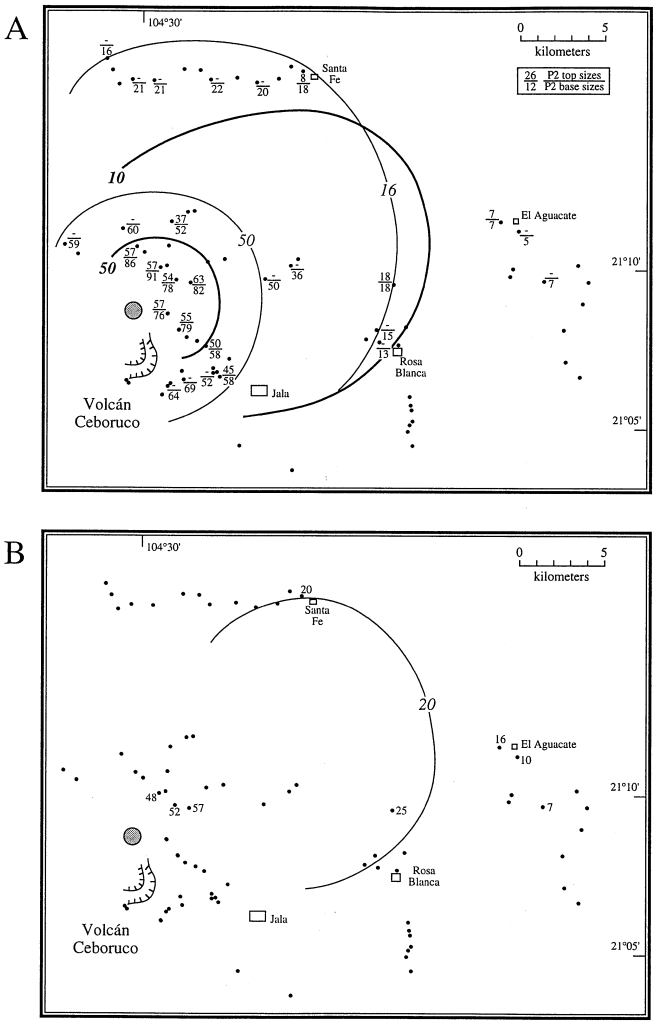


**Fig. 7** Lithic isopleths (in millimeters) for **A** the lower unit (*thin lines*) and upper unit (*thick lines*) of the P2, and **B** for the combined P3/4 layer. *Dash* indicates that measurements were not made. All data are averages of the five largest lithic fragments at each site. Possible location of the Plinian vent is shown by *stippled circle* (see text)

or soil formation (Fig. 6). Despite the few complete sections, it is clear that P3/4 was dispersed similarly to P2. The lower P3 fall deposit has a coarse base and is normally graded, whereas P4 is reversely graded and a relatively lithic-rich top. The coarsest lithics at the base of P3 are equal in size to those at the top of P4. Lithic content in P3 decreases up section from ~30 to ~20%, whereas lithic content in P4 increases from ~20 to ~50% at top. At proximal sites, the base of P3 is ~10% finer grained than the top unit of P2, whereas at more distal sites P3/4 is almost twice as coarse as the top of P2 (Fig. 7). This suggests that similar-sized material was dispersed further downwind than across wind in P3/4 relative to P2.

## P5 and P6 fall layers

Near the volcano, the next two fall deposits, P5 and P6, are separated by a thick pyroclastic flow deposit, F3, and distally by co-ignimbrite ash fall associated with F3 (Fig. 2). These fall layers are found only sporadically distally, mainly to the east of the volcano (Fig. 6). Although their distributions cannot be constrained very well, P5 and P6 appear to have been dispersed more easterly than P3/4. P5 and P6 also appear to be as lithic-rich yet finer grained as P2 and P3/4, although neither lithic sizes nor content were measured.

## Pyroclastic surge layers (S1, S2, S3)

Based on criteria discussed above, we believe that at least three of the ash layers in the Jala pumice sequence were deposited by pyroclastic surges (Fig. 2). S1 is a gray to olive-gray layer that overlies P1 at sites within 7–8 km of Volcán Ceboruco, and is thickest to the north and east (Fig. 8). S1 is also found at two distal sites, 25–30 km to the east of the summit. At a site approximately 1.5 km east of the outer caldera rim, S1 thickens from ~7 to over 80 cm in 5 m along strike. Its full thickness is not known because of partial erosion by the S2 surge. Where thick, S1 contains several lenses of coarse, angular to sub-rounded pumices. S2 is a pinkish gray ash layer that overlies P2 at many sites and appears to be distributed in two lobes, one to the northeast and the other almost due east (Fig. 8). At many proximal sites, S2 is stratified, with millimeter- to centimeter-thick bands of silty ash alternating with bands of sandy ash and pumice (Fig. 5). Stratification is strongest where S2 is thickest, and at a couple of those sites it is cross bedded. S3 is a pinkish-gray ash layer that separates P3/4 at localities within 5 km of the volcano (Fig. 2). S3 grades laterally from a stratified and, sometimes, crossbedded unit near the volcano to a massive band of ash that coats pumices and lithics (Fig. 5). Although S3 has been recognized at only a few localities, it clearly thins with distance away from the volcano (Fig. 9).

## Pyroclastic flow layers

Overlying P3/4 are two irregularly dispersed pyroclastic flow deposits, F1 and F2 (Fig. 2). F1 is up to 50 cm thick and internally stratified, with largest lithic fragments at its base and largest pumices at its top. F1 also has a thin (up to 14 cm) lithic-rich breccia at its base. F2 is up to 76 cm thick and consists of two reversely graded units. These units grade laterally to a combined thickness of 10–30 cm, where they are dark gray and weakly stratified (Fig. 10). F3, where it is thicker than 1 m, is rich in pinkish gray ash with imbricated pumice and lithic fragments. This layer varies in thickness similarly to F1/2 (Fig. 10). F4, a

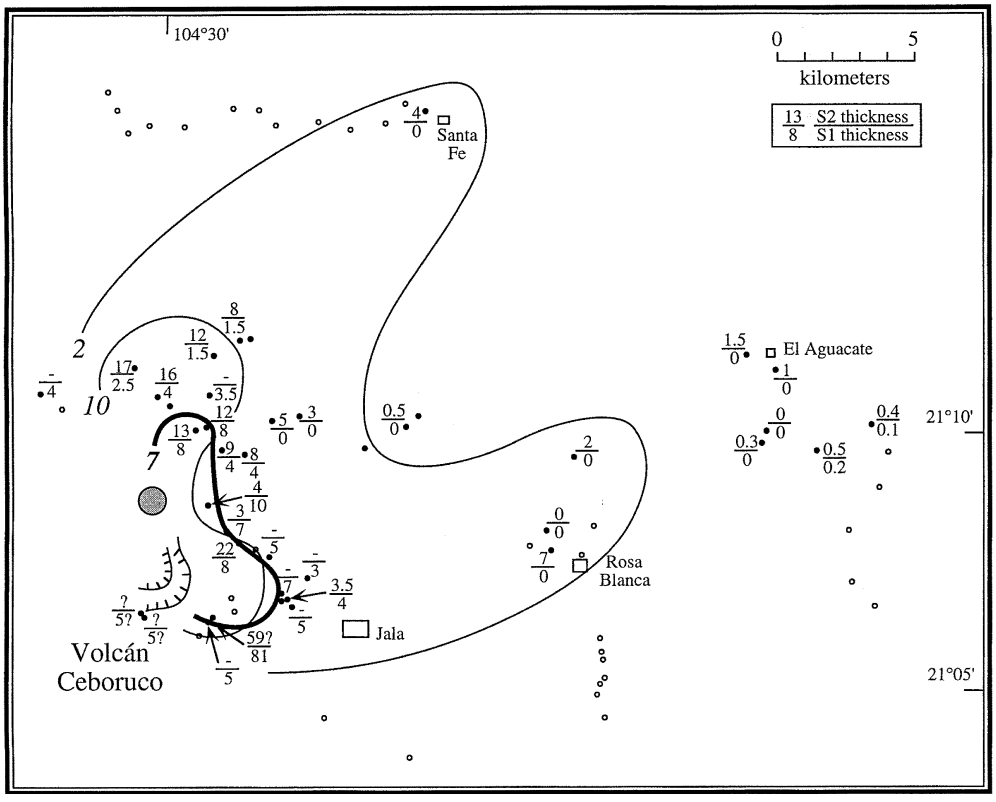


**Fig. 8** Isopachs (in centimeters) of S1 pyroclastic surge deposit (*thick line*) and S2 pyroclastic surge deposit (*thin lines*). Sites where either layer is found are shown by *filled circles*; *Dashes* are where S2 is absent as a result of erosion. Queries indicate uncertain correlation. A zero thickness indicates that S1 or S2 was not found, although its stratigraphic position is present in the exposed tephra sequence. Possible location of the Plinian vent is shown by *stippled circle* (see text)

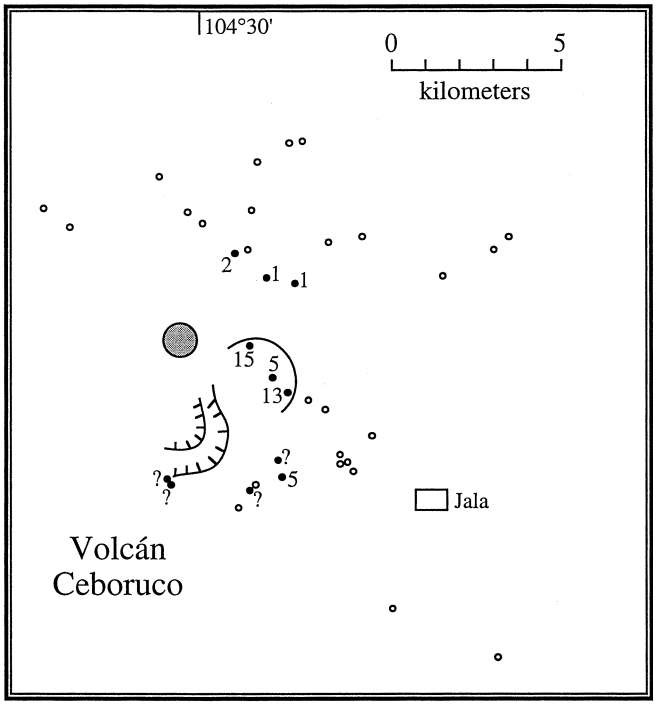


**Fig. 9** Thicknesses (in centimeters) of S3 pyroclastic surge deposit. *Filled circles* are sites where the S3 was found. *Sites outlined* are where S3 is stratified. *Queries* indicate where a deposit exists but correlation is uncertain. Possible location of the Plinian vent is shown by *stippled circle* (see text)

pinkish gray ash layer that overlies P6 near the volcano (Fig. 2), is up to 3 m thick on the northern flanks of Ceboruco. F4 is overlain by up to three thin ash layers and four well-sorted fall layers, some of which are very rich in lithics (Fig. 2). Nelson (1980) discussed a site north of volcano where he found a thick, poorly sorted, massive ash layer, overlain by several ash-rich and lithic-rich layers. Those layers probably correlate to F4 and the overlying ash and lithic layers, suggesting that F4 was deposited at least to the north.

The Marquesado pyroclastic flow deposit, exposed south and west of the volcano, is almost certainly related to the eruption of the Jala pumice (Nelson 1980). The deposit is composed of at least two flow units, separated by a 3- to 5-m-thick lithic breccia. The upper flow is overlain by several alternating layers of pumice fall and ash. Nelson (1980) correlated those fall and ash layers to the main part of the Jala pumice (i.e., P1 and above). This implied that the Marquesado pyroclastic flow was erupted first in the sequence. Instead, we suggest that the Marquesado flows erupted late in the sequence, based on two observations. Firstly, where the base of P1 is exposed on the southern slopes of Ceboruco, it overlies lava blocks and soil, rather than any ash deposit (pyroclastic flow or co-ignimbrite fall). It seems unlikely that the Marquesado pyroclastic flows could erupt to the south and leave no trace on the volcano's southern flanks. Secondly, a preliminary examination of pumices from the Marquesado flow deposits revealed that

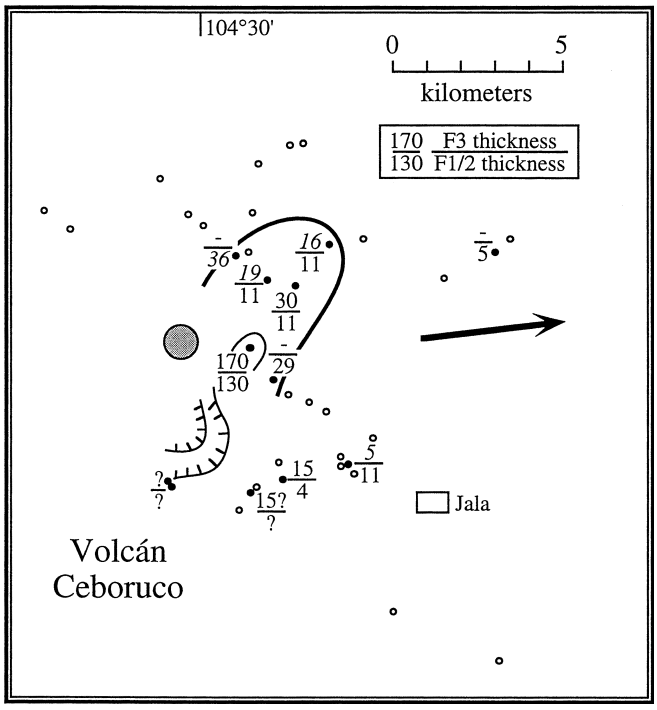


**Fig. 10** Thicknesses (in centimeters) of the combined F1 and F2 pyroclastic flow deposits (*lower numbers*) and for F3 pyroclastic flow deposit (*upper numbers*). *Dash* indicates where F3 is absent. *Italicized numbers* indicate where deposit is incomplete. The *thick line* encloses where F1/2 were deposited directly from flows. The *thin line* encloses where F3 was deposited directly from a flow. Other sites are probably co-ignimbrite ash falls, all dispersed in a direction indicated by the *arrow*. Queries indicate where similar deposits exist but correlation is uncertain. Possible location of the Plinian vent is shown by *stippled circle* (see text)

the proportion of gray pumices is similar to those in the upper (post P1) fall layers, and significantly more than in P1. A significant amount of gray pumices indicates that the Marquesado deposit erupted after P1, not before. It seems most likely that the Marquesado pyroclastic flows erupted late in the sequence and correlate with any or all of the ash layers that overlie P1.

## Erupted volume of the Jala pumice

Nelson (1980) estimated that the total tephra volume of the Jala pumice is approximately 5 $km^3$, yet he recognized that this was an underestimate because it only roughly estimated the volume of ash deposited outside of his study area. Indeed, it has now been established that a large fraction of tephra ejected during Plinian eruptions is dispersed far down wind (Sarna-Wojcicki et al. 1981; Pyle 1989, 1995; Fierstein and Nathenson 1992). Thickness isopachs for many of the fall layers were constructed in order to estimate volumes, using a model that attempts to better constrain the volume of distal ash (Table 2). The method used is based on that of Pyle (1989) which utilizes the exponential decay in deposit thickness by plotting data on graphs of ln (thickness) vs (isopach area)$^{1/2}$. Many deposits display two curves on such plots, one defined by proximal data and the other by distal data, with much of the volume encompassed by the distal curve (Pyle 1989, 1995; Fierstein and Nathenson 1992). Our measurements are from only the proximal region around Volcán Ceboruco and thus do not represent their full volumes. Total volumes were therefore calculated using the method of Carey et al. (1995) which modified that of Pyle (1989) by scaling proximal data to other Plinian-fall deposits for which more widespread thickness measurements are available.

**Table 2** Pyroclastic layers in the Jala pumice deposit of Volcán Ceboruco. – not determined; n.a. not applicable

| Tephra layer | Type[a] | Dispersal axis[b] | Tephra volume ($km^3$)[c] | Magma volume ($km^3$)[c] | Column height (km)[d] | Intensity ($kg\ s^{-1}$)[d] |
|---|---|---|---|---|---|---|
| P0 | Fall | N35 °E | 0.04 | 0.01 | < 10 | $< 10^6$ |
| P1 | Fall | N70°E | 8 – 9 | 2.5 – 3 | 30 | $8 \times 10^7$ |
| S1 | Surge | N and E | 0.004 | 0.002 | n.a. | – |
| P2 (basal unit) | Fall | N55 °E | 1.1 – 1.3 | 0.2 – 0.3 | 31 | $1 \times 10^8$ |
| P2 (reverse unit) | Fall | N50 – 60 °E | 0.5 – 0.6 | 0.11 – 0.13 | 22 | $2 \times 10^7$ |
| S2 | Surge | NE and E | 0.009 | 0.005 | n.a. | – |
| P3/4 | Fall | N45 °E | 0.4 – 0.5 | 0.1 – 0.3 | 20 – 25 | $1 – 4 \times 10^7$ |
| S3 | Surge | NE | – | – | n.a. | – |
| F1/2 | Flow | NE and E | – | – | n.a. | – |
| P5/6 | Fall | ENE | – | – | n.a. | – |
| F3 | Flow | NE(?) | – | – | n.a. | – |
| F4 | Flow | NE(?) | – | – | n.a. | – |
| Marquesado | Flow | S and SE | 0.2 | 0.12 – 0.16 | n.a. | – |

[a] Pyroclastic fall, surge, or flow
[b] Axes from isopachs; only approximate directions are available for surges and flows. (?) Very poorly constrained dispersal
[c] Tephra volumes estimated from isopachs. Magma volumes calculated assuming density deposit of 900 kg $m^3$, magma density of 2500 kg $m^3$, and subtracting lithic contents
[d] Column height for fall layers calculated from lithic isopleths using model of Carey and Sparks (1986). Intensities (mass eruption rate) calculated from the model of Sparks (1986) using estimated column heights, a temperature of 850 °C, and a tropical atmopheric profile

Layer P0 thins substantially in our study area (Fig. 3), and so we assume that extrapolation of our data reasonably approximates the volume erupted. We estimate that ~0.04 $km^3$ of tephra was dispersed in P0. Layer P1, by far the thickest fall layer in the Jala pumice (Fig. 3), consists of 8–9 $km^3$ of tephra. Layer P2 is composed of 1.5–2 $km^3$ of tephra, approximately 60% of which is the lower unit. Finally, we estimate that layer P3/4 represents 0.4–0.5 $km^3$ of tephra, although isopachs for this layer are not well constrained (Fig. 5). We have too little data to estimate volumes for the other fall layers.

The volumes of magma erupted (dense-rock equivalents, DRE) were calculated from tephra volumes (Table 2). Firstly, the amount of accidental lithic material in each layer was subtracted, using the sieve data to estimate lithic contents of each layer. Because our sieve samples came from a proximal site, the proportion of lithics are overestimated, and thus magma volumes are conservative. For P0, which was not sieved, we assume that it, like P1, contains 8% lithics. Once lithic volumes were subtracted, the remaining juvenile (pumice and ash) volume was converted to DRE assuming a tephra density of 900 kg $m^{-3}$ and a magma density of 2500 kg $m^{-3}$ (Table 2). The Marquesado pyroclastic flow deposit is the most voluminous of the flow and surge deposits. Nelson (1980) estimated that its volume is approximately 0.2 $km^3$, which suggests a magma volume of 0.12–0.16 $km^3$ (20–40% lithics; Nelson 1980). The volumes of S1 and S2 are approximately 0.004 and 0.009 $km^3$ (0.002 and 0.005 $km^3$ DRE), respectively, but these are poorly constrained. The distributions of S3 and F1–F4 are not constrained enough to estimate their volumes. It seems reasonable that 0.14 and 0.18 $km^3$ of magma erupted during the Jala pumice event was deposited as pyroclastic flows and surges. Most co-ignimbrite and co-surge ash fall have not, however, been taken into account.

In all, the Jala pumice and Marquesado pyroclastic flow deposits represent the eruption of 3–4 $km^3$ of magma. This volume is similar in magnitude to those ejected during the eruptions of Vesuvius in 79 AD and Volcán Quizapu in 1932 (Carey and Sigurdsson 1987; Hildreth and Drake 1992). Most interestingly, more than 90% of the 3–4 $km^3$ was erupted in Plinian-style columns, despite the generation of a caldera during the eruption.

## Plume heights and eruption dynamics during the Jala pumice

The areal distributions of lithic sizes in the fall layers were contoured (isopleths) in order to estimate column height of the eruption plumes from the dispersal model of Carey and Sparks (1986). Carey et al. (1990) used that model to calculate the height of the eruption cloud produced by the 18 May 1980 Plinian eruption of Mount St. Helens at different times during the day. They showed that those heights agree to within 10% of radar measurements made of the plume, and thus we assume that the heights estimated in this study have an error of ±10%. We did not calculate wind speeds form the Carey and Sparks (1986) model, because the vertical variation of wind velocity with height must be known in order to calculate wind speeds from isopleths. Not knowing wind speed does not affect the estimate for column height.

Isopleths for layer P0 are very elongated (Fig. 4). Their narrowness implies that the plume was low in height, almost certainly less than 10 km. The extreme elongation also suggests that the P0 plume was dispersed by strong winds (Carey and Sparks 1986). The very slight size grading in P0 shows that plume height was relatively stable.

Relative changes in plume height during deposition of P1 was determined by constructing isopleths for the base, coarsest, and top layers of the deposit (Fig. 4). This assumes that these levels are everywhere isochronous. Because most outcrops of the deposit record similar grain-size variations, this indicates that most of the outcrops received deposition throughout the eruption. It could be argued that deposition at a given level in a deposit cannot be isochronous everywhere because fallout should occur at proximal sites before distal sites. Although true, the difference will basically be the time it takes a particle to travel in the eruption plume to a distal locality after a particle is deposited proximally (rise and fall times being approximately equal). The farthest distance between sites is 31 km; thus, if wind speed were 30 m $s^{-1}$ (like those during the 1980 eruption of Mount St. Helens; Sarna-Wojcicki et al. 1981), the difference in time would be approximately 17 min, which is short compared with the likely length of the eruption. At sites where the fine-grained top of P1 is missing or where the deposit was not subdivided, we assume that the lithics measured are from the coarse level.

Isopleths for the base and top (below the fine-grained level) of P1 give plume heights of 25 and 26 km, indistinguishable given the errors in the method. Isopleths for the coarsest level of P1 give an average plume height of 30 km, which, given the errors in the method, is similar to those estimated for the other levels of the deposit. Changes in areas covered by given isopleths between the different levels of P1 indicate, however, that plume height did vary during that phase of the eruption and reached its peak during deposition of the coarsest level. Clearly, however, the variations were relatively small. Lithic isopleths were constructed for the lower unit of P2 (Fig. 7), and their distribution implies deposition from a plume that was 31 km high. Weak normal grading suggests that plume height decreased slightly during deposition of this unit. In the upper unit of P2, lithic isopleths for the top of the unit give a plume height of 22 km (Fig. 7). This unit is strongly reversely graded, with maximum lithic

sizes at its base being equal in size to those in P0. This suggests that plume height had dropped significantly across the transition from the lower to upper units, and then plume height increased significantly. Roughly, the few measured lithic sizes in P3/4 (Fig. 7) suggest a plume height of 20–25 km. Height probably varied during deposition of P3/4, because P3 is normally graded and P4 is reversely graded.

The height of an eruption plume is related to the mass eruption rate (intensity) of the eruption (Sparks 1986; Woods 1988). We calculated intensities from our estimated column heights, using the model curves of Sparks (1986) derived for a tropical climate (Table 2). The low plume height for P0 means that intensity was probably less than $10^6$ kg $s^{-1}$ (Table 2). During P1, intensity varied between $4 \times 10^7$ and $8 \times 10^7$ kg $s^{-1}$. Peak intensities of $10^8$ and $2 \times 10^7$ kg $s^{-1}$ were reached during deposition of the lower and upper units of P2, although variations in grain size clearly show that intensity varied significantly during this phase of the eruption, and possibly as much as the difference between P0 and P1. An intensity of $1–4 \times 10^7$ kg $s^{-1}$ was reached during P3/4, similar to the end of P2.

## Magmas of the eruption

Two magmas were tapped during the Jala pumice eruption, one rhyodacitic (white pumice) and the other dacitic (gray pumices; Table 1). Banded pumices record intimate mixing between the two. Herein we discuss the proportions of the two magmas erupted and highlight some important differences. A full discussion is beyond the scope of this study and will be the subject of a subsequent paper.

Based on deposit volumes and the relative amounts of white and gray pumices in those layers, approximately 2.7–3.4 $km^3$ of rhyodacite and 0.2–0.3 $km^3$ of dacite were erupted in P1, P2, and P3/4. A preliminary search in the Marquesado pyroclastic flow showed that a significant proportion were gray pumices, like the upper fall layers. Assuming 30% gray pumices, we estimate that 0.09–0.12 $km^3$ of rhyodacite and 0.04–0.05 $km^3$ of dacite erupted as pyroclastic surges and flows. Therefore, of the 3–4 $km^3$ of magma erupted, 2.8–3.5 $km^3$ was rhyodacite and 0.2–0.5 $km^3$ was dacite. Variations in proportions indicate that, although both magmas were tapped continuously, more than 85% of the rhyodacite erupted during P1, whereas more than 70% of the dacite erupted after P1.

Rhyodacite pumices are homogenous in composition (Table 1), and are composed of highly vesicular rhyodacitic glass and $<1$ vol.% plagioclase, orthopyroxene, magnetite, and ilmenite (Nelson 1980). Magnetite–ilmenite pairs in the rhyodacite are compositionally unzoned and give temperatures of $\sim 865\,^{\circ}C$, using the Andersen and Lindsley (1988) algorithm. Dacite pumices, which were not mentioned by Nelson (1980), are also relatively homogenous (Table 1). Phenocrysts include plagioclase, clinopyroxene, orthopyroxene, hornblende, magnetite, ilmenite, and olivine, all set in a vesicular, microlite-rich groundmass.

Many of the phenocrysts have compositions that equal those in the rhyodacite. Olivine, clinopyroxene, and hornblende phenocrysts are unique to the dacite, but are all rimmed with reaction zones, variably composed of plagioclase, pyroxene, Fe–Ti oxides, and glass (hornblende reaction rims also contain olivine). Magnetite–ilmenite pairs give a spread in temperature from $\sim 865$ to $\sim 1030\,^{\circ}C$. We believe that the dacite magma is a hybrid between the rhyodacite magma and a more basic magma (represented by olivine, clinopyroxene, and hornblende phenocrysts and high-temperature Fe–Ti oxides). Reaction rims suggest that mixing occurred long before erupting. Some rhyodacitic phenocrysts in the dacite are unzoned, however, suggesting that they were incorporated either during or just before the eruption. We suggest that a two layered reservoir existed beneath Ceboruco at the time of eruption, a homogenous rhyodacite layer and a hybrid dacite layer, formed by mixing between rhyodacitic and more basic magmas.

## Discussion

In this section we reconstruct some important characteristics of the eruption sequence based on our tephrostratigraphy, and discuss the broader implications for current understanding of caldera-forming eruptions. After discussing probable locations of the eruption vents, we assess the evolution of the mass flux during the eruption and how the eruption sequence and caldera collapse can be linked. In contrast to many caldera-forming eruptions, most of the magma erupted during the Jala pumice event was deposited as fall layers from Plinian eruption columns. The combined volumes of fall layers P0–P4 is 2.9–3.7 $km^3$ (DRE), whereas less than 0.2 $km^3$ (DRE) was deposited as pyroclastic flows and surges.

The Jala pumice eruption vent does not appear to be exposed, but we can infer its location from the distribution of Plinian deposits. At most localities the top of the P1 deposit was eroded only a few centimeters by the S1 surge; thus, measured thicknesses represent true thicknesses. Isopachs of P1 do not extrapolate toward the summit of the volcano, but rather to its northern flanks (Fig. 3). Lithic isopleths of P1 are also displaced to the north (Fig. 4). Isopachs and isopleths for P2 also extrapolate to the northern flanks (Figs. 6, 7), and, although less well constrained, data for P0 and for P3/4 also point to the same area. Thus, all of the Plinian fall layers of the Jala pumice plausibly erupted from a vent located to the north of the caldera. This vent is buried now by the El Norte lava flow (Fig. 1). Vents for the pyroclastic flows and surges are less certain, yet the double-lobed form of the isopachs

of S1 and S2 (Fig. 8) possibly suggests that other vents were involved.

One striking observation is that the top of P1 is much finer grained than the bulk of P1 and is similar in grain size to P0 (Fig. 5). Unlike P0, which has narrow, lobate isopachs, suggesting deposition from a low, sub-Plinian column in relatively strong winds, the fine-grained, pumice-rich top of P1 is broadly distributed and decreases in thickness slowly as a function of distance from the vent (Fig. 3). We interpret this to mean that the fine-grained top was deposited from an umbrella cloud of similar extent to that responsible for the deposition of most of P1, but that the eruption decreased substantially in intensity at the end of the deposition of P1. This drop in intensity would lead to much of the fine-grained material being deposited much closer to the volcano than would have occurred if conditions had remained steady in the umbrella cloud. In short, the eruption flux from the Plinian vent decreased tremendously or conceivably even briefly stopped at the stage of the eruption when fine pumice at the top of P1 was deposited. The upper, lithic-rich part of the fine-grained top of P1 has a distribution very similar to that of P0 (Fig. 3). This suggests that after the dramatic decrease in eruption intensity, a relatively low, sub-Plinian eruption column was re-established, much like that which deposited the P0 layer. It seems reasonable to conclude that the pressure differential driving the eruption had decreased substantially at the end of P1, but following eruption of the S1 surge, a Plinian column (P2) was re-established with a column height and mass flux very similar to that of the main P1 phase (Table 2). That the eruption could resume in this way is important evidence for how the system was evolving mechanically as magma was extracted. There is evidence that this kind of hiatus in an eruption sequence also occurred in other caldera-forming events, e.g., the 1912 eruption of Mt. Katmai (Fierstein and Hildreth 1992).

Despite similarities in peak column heights and intensities, there are significant differences between the P1 and P2 phases. Firstly, there are large variations in sizes and grading of lithics in P2. Isopleth shapes show that these variations did not result from shifting winds, and thus there must have been large variations in mass flux during P2 despite its much smaller volume and shorter duration. Therefore, the eruption column was less stable during P2 relative to P1. Secondly, there are substantially more lithics in P2 than in P1. This difference cannot be attributed to a change in deposition; it means that the proportion of lithics relative to magma in the erupting mixture was much higher during the P2 phase. It is probable that the two differences are related, because the introduction of more lithics into the erupting mixture, as a result of changing conduit erosion or collapsing conduit walls, could cause less stable behavior of the column during the P2 phase.

The P2 layer is capped, like P1, by a surge deposit (S2), but unlike the top of P1 the top of P2 is reversely graded, implying that mass flux increased up to when S2 erupted. This may mean that either the Plinian eruption column was stable and that S2 erupted from a separate vent, or that the column collapsed. We cannot easily differentiate between the two possibilities, but we do note that mass flux for the P3 phase was similar to that at the end of P2. This suggests that if S2 were generated by collapse, it could only be partial collapse of an otherwise stable column.

The Jala pumice eruption appears, therefore, to have occurred in two phases. The first phase saw a sustained Plinian column (P1), during which 2.5–3 $km^3$ of magma erupted. This phase apparently ended abruptly (top of P1) and was followed by alternating Plinian columns and pyroclastic surges and flows, during which 0.5–0.9 $km^3$ of magma erupted. Mass flux and lithic abundance during this second phase were highly variable, compared with the first phase. The end of the P1 phase also marks an abrupt change in the composition of erupting magma. During P1, rhyodacite erupted and very little dacite was tapped, whereas subsequently significant proportions of dacite were erupted.

## Caldera formation

Nelson (1980) reasonably argued that the larger, outer caldera of Volcán Ceboruco formed when the Jala pumice erupted, mainly because that deposit is the uppermost one found on the caldera rim and no Jala pumice deposits are found inside the caldera. Much of the caldera has been obscured by later erupted lavas and domes, but Nelson (1980) estimated that its volume was approximately 3.4 $km^3$. We calculate that 3–4 $km^3$ of magma erupted during the Jala pumice event. Nelson (1980) deduced the collapse volume by assuming that the pre-caldera volcano was conical, that the caldera was circular (3.7 km in diameter), and that collapse was on average 250 m. A conical shape is probably the least tenable of these assumptions. If we instead assume that the volcano was flat topped, then collapse of a 250-m-deep cylinder is 2.8 $km^3$. This is still comparable to the total erupted magma and substantially larger than that erupted after P1 (Table 2).

The coincidence of significant changes in the eruption occurring at approximately the P1–P2 boundary may likely reflect onset of collapse. This is, however, difficult to fit into a general model for caldera formation because of the above volume relationships. It is commonly thought that eruptions commence when overpressure builds in a magma chamber and forms a crack that propagates to the surface. Reasonable assumptions about the release of overpressure from a chamber in elastic country rocks indicate that a volume of magma corresponding to only a relatively small fraction of the chamber can be vented before

the overpressure is released (e.g., Tait et al. 1989). One model for caldera-forming events holds that once enough magma has vented to release the overpressure, continued eruption of magma then underpressurizes the chamber, removing support for the roof, and caldera collapse begins (Druitt and Sparks 1984). Collapse of the dense roof into less dense magma then drives out a large proportion of magma from the chamber and hence a volume of magma typically much larger than that vented during the overpressured phase. This model seems to fit cases in which a Plinian phase was followed by venting of substantially larger volumes of pyroclastic flows, e.g., the Minoan eruption of Santorini volcano (Bond and Sparks 1976) and the climactic eruption of Mount Mazama (Bacon 1983). This model does not explain our observations, however, because if P0–P1 layers represent the "overpressured" phase and the onset of caldera formation began at the P1–P2 boundary, then the amount of magma erupted during the overpressured phase is approximately three times more voluminous than that erupted during caldera collapse. It cannot be argued within the above framework that the Ceboruco magma chamber was emptied, because the "overpressure" volume (P0 and P1) cannot be more voluminous than the remaining magma body (represented by the other tephra layers). On the other hand, the caldera could have started to collapse near to the beginning of the eruption. While this interpretation would explain why the total volume of the Jala pumice corresponds closely to that of the caldera, it does not appear to fit the assumption that caldera formation begins when the reservoir becomes underpressurized (Druitt and Sparks 1984), because the deposits show no sign of a transition from overpressure to underpressure early in the P1 part of the sequence; the P1 column was sustained and stable.

It is admittedly hard to unambiguously place caldera collapse in the Jala pumice eruption sequence, but we conclude that the most probable point is near the end of the eruption of the P1 layer. This suggests to us that existing mechanical models of caldera collapse do not provide a good explanation for this and, possibly, other similar deposits. Models have mostly been constructed in order to explain the formation of calderas at least an order of magnitude larger in volume than that of Ceboruco, and there may be some differences in the mechanics that depend on size. If our observations from Ceboruco are typical of relatively small caldera-forming eruptions, it would be a hint that the above framework does not provide a general model for caldera collapse.

**Acknowledgements** We thank S. Nelson, J. Luhr, P. Wallace, and D. Snyder for help and advice with field logistics at Volcán Ceboruco. We also thank J. Devine for help with whole-rock fusions and electron microprobe analyses. Insightful reviews by J. Fierstein, H. Kamata, and S. Nelson greatly improved the manuscript. This research was supported partially by NSF grant EAR-9526527 and by EC project ENV4-CT97-0703.

## References

Andersen DJ, Lindsley DH (1988) Internally consistent solution models for Fe–Mg–Mn–Ti oxides: Fe–Ti oxides. Am Mineral 73:714–726

Andersen DJ, Lindsley DH, Davidson PM (1993) QUILF: a Pascal program to assess equilibria among Fe–Mg–Ti oxides, pyroxenes, olivine, and quartz. Comput Geosci 19:1333–1350

Bacon CR (1983) Eruptive history of Mount Mazama and Crater Lake caldera, Cascade Range, USA. J Volcanol Geotherm Res 18:57–115

Bond A, Sparks RSJ (1976) The Minoan eruption of Santorini, Greece. J Geol Soc Lond 312:1–16

Carey S, Sigurdsson H (1987) Temporal variations in column height and magma discharge rate during the 79 A.D. eruption of Vesuvius. Geol Soc Am Bull 99:303–314

Carey S, Sparks RSJ (1986) Quantitative models of fallout and dispersal of tephra from volcanic eruption columns. Bull Volcanol 48:109–125

Carey S, Sigurdsson H, Gardner J, Criswell W (1990) Variations in column height and magma discharge during the May 18, 1980 eruption of Mount St. Helens. J Volcanol Geotherm Res 43:99–112

Carey S, Gardner J, Sigurdsson H (1995) The intensity and magnitude of Holocene Plinian eruptions from Mount St. Helens volcano. J Volcanol Geotherm Res 66:185–202

Devine JD, Gardner JE, Brack HP, Layne GD, Rutherford MJ (1995) Comparison of microanalytical methods for estimating $H_2O$ contents of silicic volcanic glasses. Am Mineral 80:319–328

Druitt TH, Francaviglia V (1992) Caldera formation on Santorini and the physiography of the islands in the late Bronze Age. Bull Volcanol 54:484–493

Druitt TH, Sparks RSJ (1984) On the formation of calderas during ignimbrite eruptions. Nature 310:679–681

Fierstein J, Hildreth W (1992) The Plinian eruptions of 1912 at Novarupta, Katmai National Park, Alaska. Bull Volcanol 54:646–684

Fierstein J, Nathenson M (1992) Another look at the calculation of fallout tephra volumes. Bull Volcanol 54:56–167

Hildreth W (1991) The timing of caldera collapse at Mount Katmai in response to magma withdrawal toward Novarupta. Geophys Res Lett 18:1541–1544

Hildreth W, Drake RE (1992) Volcán Quizapu, Chilean Andes. Bull Volcanol 54:93–125

Lipman P, Dungan M, Bachman O (1997) Comagmatic granophyric granite in the Fish Canyon Tuff, Colorado: implications for magma-chamber processes during a large ash-flow eruption. Geology 25:915–918

Nelson SA (1980) Geology and petrology of Volcán Ceboruco, Nayarit, Mexico. Bull Geol Soc Am 91:2290–2431

Paladio-Melosantos LO, Solidum RU, Scott WE, Quiambao RB, Umbal JV, Rodolfo KS, Tubianosa BS, Delos Reyes PJ, Alonso RA, Ruelo HF (1996) Tephra falls of the 1991 eruptions of Mount Pinatubo. In Newhall CG, Punongbayan RS (eds) Fire and mud: eruptions and lahars of Mount Pinatubo, Philippines. Univ Wash Press, Seattle, pp 513–536

Pyle DM (1989) The thickness, volume and grain size of tephra fall deposits. Bull Volcanol 51:1–15

Pyle DM (1995) Assessment of the minimum volume of tephra fall deposits. J Volcanol Geotherm Res 69:379–382

Sarna-Wojcicki A, Shipley S, Waitt RB, Dzurisin D, Wood SH (1981) Aerial distribution, thickness, mass, volume, and grain size of air-fall ash from the six major eruptions of 1980. US Geol Surv Prof Pap 1250:577–600

Sigurdsson H, Carey S, Mandeville C (1991) Krakatau, submarine pyroclastic flows of 1883 eruption. Nat Geogr Res Explor 7:310–327

Smith RL (1960) Ash flows. Bull Geol Soc Am 71:795–842

Smith RL (1979) Ash-flow magmatism. Geol Soc Am Spec Pap 180:5–27

Smith RL, Bailey RA (1968) Resurgent cauldrons. Geol Soc Am Mem 116 : 613–662

Sparks RSJ (1986) The dimensions and dynamics of volcanic eruption columns. Bull Volcanol 48 : 3–16

Steven TA, Lipman PW (1976) Calderas of the San Juan volcanic field, southwestern Colorado. US Geol Surv Prof Pap 958 : 1–35

Suzuki-Kamata K, Kamata H, Bacon CR (1993) Evolution of the caldera-forming eruption at Crater Lake, Oregon, indicated by component analysis of lithic fragments. J Geophys Res 98 : 14059–14074

Tait S, Jaupart C, Vergniolle S (1989) Pressure, gas content and eruption periodicity of a shallow, crystallizing magma chamber. Earth Planet Sci Lett 92 : 107–123

Williams H (1941) Calderas and their origin. Calif Publ Bull Dept Geol Sci 25 : 239–346

Williams SN, Self S (1983) The October 1902 Plinian eruption of Santa María volcano, Guatemala. J Volcanol Geotherm Res 16 : 33–56

Woods AW (1988) The fluid dynamics and thermodynamics of eruption columns. Bull Volcanol 50 : 169–193